

PACS numbers: 52.50.Jm; 52.25.Qt
DOI: 10.1070/QE2000v030n10ABEH001829

Optical characteristics of the near-surface plasma initiated by high-power femtosecond laser pulses of different polarisation

V M Velichko, V D Urlin, B P Yakutov

Abstract. The interaction of differently polarised femtosecond laser pulses with an intensity of $10^{15} - 10^{17}$ W cm^{-2} with the surface of a solid target was calculated theoretically. In the calculation of absorption of the laser radiation, the electrodynamic, hydrodynamic, and kinetic equations were solved in combination at the plasma – vacuum boundary. The dependences of plasma reflectivity on the intensity, polarisation, and the angle of incidence of laser radiation on the target were determined. A comparison with experimental data was made.

1. Introduction

Recently laser radiation sources with the pulse duration $\tau \sim 10^{-14} - 10^{-13}$ s have been developed, which are capable of producing light fields of the intensity $I \sim 10^{16} - 10^{20}$ W cm^{-2} [1, 2]. The irradiation of targets by laser pulses with such parameters produces a thin ($\sim 0.1 - 1$ μm) plasma layer of the solid-state density ($n_{e,i} \sim 10^{22} - 10^{23}$ cm^{-3}) with the electron temperature $T_e \sim 0.5 - 1$ keV and 'cold' ions. This superdense hot near-surface plasma is a unique physical object whose properties are actively investigated [1, 2].

The question of the mechanism of laser radiation absorption by the near-surface plasma with such extreme parameters is very important in studies of the interaction of femtosecond laser pulses with solid targets. This question also attracts considerable attention because the plasma absorptivity and its reflectivity are among the few parameters of a femtosecond plasma that can be reliably measured in experiments [3 – 8].

The aim of this work is to calculate the optical plasma characteristics during irradiation of a solid target by a femtosecond laser pulse of arbitrary linear polarisation. The studies were made using a through-computation code in Lagrangian coordinates allowing a simultaneous numerical simulation of electrodynamic, kinetic, hydrodynamic, and radiative processes in a laser-produced plasma. We used a model of plasma permittivity that allowed us to adequately describe the absorption of femtosecond laser pulses of the intensity $I \leqslant 10^{17}$ W cm^{-2}. The results of calculations of the optical plasma parameters were compared with the experimental results reported in the literature.

V M Velichko, V D Urlin, B P Yakutov All-Russian Federal Nuclear Centre (All-Russian Research Institute of Experimental Physics), prosp. Mira 37, 607190 Sarov, Nizhnii Novgorod oblast, Russia

Received 10 March 1999; revision received 29 September 1999
Kvantovaya Elektronika **30** (10) 889 – 895 (2000)
Translated by E N Ragozin

2. Theoretical model and computation of the USP – target surface interaction and USP absorption

2.1. Calculation of the hydrodynamic parameters of a femtosecond plasma and its charge-state composition

The irradiation of a target by a USP has several specific features. The short ($\sim 10^{-13} - 10^{-12}$ s) time scales and high ($10^{16} - 10^{19}$ W cm^{-2}) intensities of irradiation result in strong temperature, density, and charge gradients in the produced near-surface plasma. The plasma dynamics in problems of this kind is described in the approximation of one-dimensional, two-temperature, one-liquid hydrodynamics in Lagrangian coordinates [7 – 11]. The one-dimensional nature of the approximation stems from the fact that the focal spot diameter $d \sim 10 - 100$ μm remains far greater than the thickness $L_p \sim 0.1 - 1$ μm of the plasma produced by a femtosecond laser pulse at the target surface.

The method of calculation in use allows us to take into account, apart from the hydrodynamic plasma motion, such phenomena as the absorption of laser radiation, the electron–ion energy exchange, the heating of target material due to the electron thermal conduction, and also the transient ionisation kinetics for the determination of the average ion charge. The equation of state of the electron component is written in the ideal gas approximation. Since the characteristic temperatures of laser-induced target heating are much higher than the vaporisation temperature of the target material, the lattice can be also treated as an ideal gas; the heat capacity of the electron gas and the lattice was taken to be equal to 3/2. The basic equations have the form:

$$\frac{\partial E_e}{\partial t} = -(P_e + P_v/2)\frac{\partial u}{\partial m} + q_e + Q_{las} - Q_{ei} - Q_{rad}, \quad (1)$$

$$\frac{\partial E_i}{\partial t} = -(P_i + P_v/2)\frac{\partial u}{\partial m} + Q_{ei}, \quad (2)$$

$$\frac{\partial u}{\partial t} = -\frac{\partial (P_e + P_i + P_v/2)}{\partial m}, \quad (3)$$

$$\frac{\partial (1/\rho)}{\partial t} = \frac{\partial u}{\partial m}, \quad (4)$$

$$\frac{\partial x}{\partial t} = u, \quad (5)$$

where u is the velocity of ions and electrons; ρ is the density of the medium; x is the Eulerian coordinate; m and t are the Lagrangian variables; $E_e = 1.5\langle Z\rangle T_e/M + U(\langle Z\rangle)/M$ and $E_i = 1.5T_i/M$ are the energies of the electron and ion components per unit mass; $\langle Z\rangle$ is the average ion charge; $U(\langle Z\rangle)$ is the energy expended to ionise the atom to the charge $\langle Z\rangle$; T_e and T_i are the electron and ion temperatures; $P_e = \rho\langle Z\rangle T_e/M$ and $P_i = \rho T_i/M$ are the electron and ion pressures; M is the atomic mass; P_v is the pressure arising from the introduction of artificial viscosity; Q_{ei}, q_e, Q_{las}, and Q_{rad} are the equation terms that describe the electron-ion energy exchange, the electron thermal conduction, the absorption of laser radiation, and the radiative energy losses, respectively.

The plasma state in the model employed is described by the average value $\langle Z\rangle$, which is justified, because the distribution over the degree of ionisation is relatively narrow [12]. The time variation of $\langle Z\rangle$ is described by the equation [11]

$$\frac{d\langle Z\rangle}{dt} = \langle Z\rangle(\upsilon_e - \upsilon_{st} - \upsilon_{ph}), \tag{6}$$

where υ_e, υ_{st}, and υ_{ph} are the rates of electron impact ionisation, three-body recombination, and photorecombination, respectively. The expressions for the rates of elementary processes were (following Refs [11, 13]) taken in the interpolation form. In the equilibrium case, at high densities we obtain the Saha formulas from Eqn (6), while for a low density and a high temperature, we arrive at the 'coronal' equilibrium.

The parameter Q_{ei}, which takes into account the relaxation of electron and ion temperatures, and the heat flux q_e transferred by electrons were described by classical expressions [11]. In this case, provision was made for heat flux limitation. The expression incorporating the source of laser energy release Q_{las} is discussed below. The parameter Q_{rad} was neglected at this stage of investigations.

The estimated contribution of radiative loss to the total energy balance during the laser radiation pulse is small and accounts for a fraction of a percent, which cannot have a significant effect on the results of simulation of other parameters. Because we consider the intensities $I \leqslant 10^{17}$ W cm^{-2} and short pulses at which the plasma has a density about that of a solid and a temperature of hundreds of electronvolts, the possible effect of light pressure on the plasma motion was neglected. The validity of this approximation will be demonstrated in the analysis of the results of calculations.

Eqns (1)–(5) were integrated in Lagrangian coordinates employing the 'crosslike' calculation scheme correct to the second order in space and to the first order in time. The heat conduction equation was solved by the sweep method using an implicit scheme in the second order in space and in the first order in time. Eqn (6) was solved at each point of the difference scheme by an explicit–implicit method. Using this calculation scheme based on Eqns (1)–(6), we simulated the hydrodynamic motion of the laser-produced plasma, the energy transfer from the absorption region inside the target, the electron–ion energy exchange, and determined the degree of ionisation in the plasma.

2.2. Calculation of the absorption of a femtosecond laser pulse

The absorptivity of the near-surface plasma produced upon the interaction of an ultrashort laser pulse with a solid target depends on the radiation intensity, the laser beam polarisation, the angle of laser beam incidence on the target, and the laser radiation wavelength. Because the depth L_p of the plasma layer during a femtosecond laser pulse is usually smaller than the laser radiation wavelength λ, $L_p \leqslant \lambda$, to determine the optical plasma characteristics, it is necessary to find the solution of the electromagnetic field equations at the plasma–vacuum interface. The use of geometrical optics approximation for such spatial scales becomes incorrect.

The USP-produced plasma is characterised by strong density, temperature, and charge-state composition gradients. For this reason, the calculation of the optical characteristics of such a plasma should involve simultaneous solution of the equations of hydro- and electrodynamics in order to determine the light field of laser radiation at the plasma–vacuum interface for real density, temperature, and charge-state composition profiles. Since the electrodynamic characteristics change on a shorter time scale than the hydrodynamic ones, the absorption of light is calculated using stationary wave equations.

The scheme of laser radiation–plasma interaction is shown in Fig. 1. For an s-polarised wave, the electric field E is directed normally to the plane of laser radiation incidence on the plasma. The electrodynamic equations can be reduced to the form whereby the electric field E of the wave, which propagates in the direction of the x-axis, is described by the single-component, one-dimensional wave equation [14]

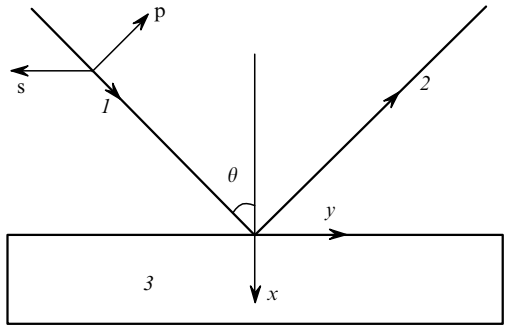

Figure 1. Scheme of the interaction of a polarised laser beam with a target: (*1*) incident beam; (*2*) reflected beam; (*3*) target.

$$\frac{d^2E}{dx^2} + k_0^2\left[\varepsilon(x) - \sin^2\theta\right]E = 0, \tag{7}$$

where $k_0 = \omega/c$; ω is the laser radiation frequency; c is the speed of light in vacuum; ε is the plasma permittivity; and θ is the angle of wave incidence on the plasma. The permittivity model accepted is discussed below.

When calculating p-polarised electromagnetic fields, we can conveniently solve the equation not for the vector E, which lies in the plane of laser radiation incidence in the case of p polarisation, but for the magnetic vector H of the wave perpendicular to the plane of beam incidence [14]. The equation describing the distribution of magnetic field of the laser radiation has the form:

$$\frac{d^2H}{dx^2} - \frac{1}{\varepsilon}\frac{d\varepsilon}{dx}\frac{dH}{dx} + k_0^2\left[\varepsilon(x) - \sin^2\theta\right]H = 0. \tag{8}$$

The coefficients in this equation have the same meaning as in Eqn (7). The x- and y-axes (see Fig. 1) lie in the plane of incidence of the laser beam, which makes an angle θ with the x-axis. The y-axis lies at the intersection of the plane of incidence of the laser beam with the plane coinciding with the initial plasma boundary. The plasma parameters depend on the coordinate x. Having determined H from Eqn (8), one can readily find, following Ref. [14], the components of the electric field E necessary for determining the absorption. The field component E_x collinear with the plasma density gradient and the field component E_y normal to the density gradient are defined by the expressions:

$$E_x = \frac{\mathrm{i}c}{\varepsilon\omega}\frac{\partial H}{\partial y}, \tag{9}$$

$$E_y = -\frac{\mathrm{i}c}{\varepsilon\omega}\frac{\partial H}{\partial x}. \tag{10}$$

The energy of the electromagnetic wave absorbed in a unit plasma volume in a unit time can be represented as [14]

$$W(x) = \omega \mathrm{Im}\,\varepsilon(x)|E(x)|^2/8\pi, \tag{11}$$

where $|E(x)|^2 = |E_x(x)|^2 + |E_y(x)|^2$ for a p-polarised wave and $|E(x)|^2 = |E_z(x)|^2$ for an s-polarised wave.

The parameter Q_{las}, which describes the laser energy release in Eqn (1), is related to $W(x)$ by the expression

$$Q_{\mathrm{las}} = \frac{W(x)}{\rho}. \tag{12}$$

Let us discuss the plasma permittivity model in more detail. As shown in Ref. [8], the choice of this model can substantially affect the results of numerical simulations of the optical plasma properties. We use here a model similar to that employed in Refs [5–9], wherein the plasma electrons and ions are treated as a gas of free particles in the electric field of laser radiation with frequency ω. In this model, the complex plasma permittivity ε is defined by the expression:

$$\varepsilon = 1 - \frac{\omega_{\mathrm{p}}^2}{\omega(\omega + \mathrm{i}\nu)}, \tag{13}$$

where $\omega_{\mathrm{p}} = (4\pi n_{\mathrm{e}} e^2/m_{\mathrm{e}})^{1/2}$ is the plasma frequency; ν is the effective frequency of electron–ion collisions which, apart from the plasma temperature and density, depends, generally speaking, on the intensity I and the frequency ω of laser radiation [14]. It was assumed in the derivation of expression (13) that the medium possesses a weak spatial dispersion, i.e., the conditions $\omega > \kappa_{\mathrm{p}}(T_{\mathrm{e}}/m_{\mathrm{e}})^{1/2}$ and $\nu > \kappa_{\mathrm{p}}(T_{\mathrm{e}}/m_{\mathrm{e}})^{1/2}$ are fulfilled, where $\kappa_{\mathrm{p}} = 2\pi/\lambda_{\mathrm{p}}$ is the wave vector of radiation in the plasma and $(T_{\mathrm{e}}/m_{\mathrm{e}})^{1/2}$ is the electron thermal velocity.

The effective electron–ion collision frequency ν is the governing quantity in expression (11) for the absorbed energy $W(x)$, because

$$\mathrm{Im}\,\varepsilon(x) = \frac{\nu\omega_{\mathrm{p}}^2}{\omega(\omega^2 + \nu^2)}. \tag{14}$$

To improve the precision of the permittivity model, we will take into account the relationship between the effective electron–ion collision frequency ν and the frequency ω of the incident electromagnetic wave. According to Ref. [9], we will assume that for $\omega > \nu$, in the so-called high-frequency limit, $\nu = \nu_{\mathrm{h}}$:

$$\nu_{\mathrm{h}} = \frac{4(2\pi)^{1/2}}{3}\frac{\langle Z\rangle e^4 n_{\mathrm{e}} \Lambda}{m_{\mathrm{e}}^{1/2} T_{\mathrm{e}}^{3/2}}, \tag{15}$$

where Λ is the Coulomb logarithm; n_{e} is the electron density of the plasma; e and m_{e} are the electron mass and charge; and T_{e} is the electron temperature.

For $\omega < \nu$, in the low-frequency limit, the dependence of ν on the temperature, the density, and the average charge remains the same, but the numerical coefficient in expression (15) is diminished by about a factor of three, so that the low-frequency effective collision frequency is

$$\nu_{\mathrm{low}} = \frac{3\pi}{32}\nu_{\mathrm{h}}. \tag{16}$$

Therefore, we described the effective collision frequency in the following way. We assume that the collision frequency is $\nu = \nu_{\mathrm{low}}$ for $\nu > \omega$, while formula (15) is valid and $\nu = \nu_{\mathrm{h}}$ for $\nu < \omega$. In the intermediate case, for $\nu \simeq \omega$, the quantities ν_{low} and ν_{h} are sewed together at the level $\nu = \omega$.

The technique of numerical solution of Eqns (7) and (8) describing the light field of the laser radiation is similar to that proposed in Ref. [6]. It is significant that Eqns (7) and (8) have exact solutions in a homogeneous medium. In a homogeneous supercritical-density plasma, these solutions are used as boundary conditions for the integration of these equations in an inhomogeneous layer. The integration of the equations proceeds outward from the plasma to vacuum. The wave reflected from the plasma and the incident wave in vacuum form a light field with the amplitude related to the current intensity of laser radiation

$$I(t) = \frac{c|E_0|^2}{8\pi}\cos\theta. \tag{17}$$

This amplitude is used to calibrate the solution and determine the plasma reflectivity R and absorptivity A. According to the energy conservation law, the equality $A + R = 1$ should be fulfilled. This equality was used to verify the precision of our calculations.

In the numerical simulation of the laser pulse–plasma interaction, Eqns (7)–(10), which describe the absorption, were solved simultaneously with the system (1)–(6). The solution yields the spatial distribution of the electric ($|E(x)|^2$) and magnetic ($|H(x)|^2$) fields, which are used to determine the reflectivity R and the spatial distribution $W(x)$ of the energy absorbed in the plasma layer.

3. Specific features of the interaction of p- and s-polarised femtosecond laser radiation with an inhomogeneous plasma

Experiments and calculations show that the absorption coefficient of p-polarised radiation exceeds, for equal intensities and angles of incidence of femtosecond laser pulses on an inhomogeneous plasma, that of s-polarised radiation [3, 4, 8]. This is caused by the resonance absorption of the p-polarised electromagnetic wave by the inhomogeneous plasma [11, 14].

Such resonance absorption will be observed if the electric vector E of the wave is collinear with the density gradient of the inhomogeneous plasma. In the calculation of absorption

of p- and s-polarised radiation, by solving Eqns (7)–(10) the magnitude of the field was determined throughout the region adjacent to the plasma–vacuum interface. In the case of p-polarised radiation, a resonance enhancement of the electric field component collinear with the density gradient occurs at the point with a critical density, and the absorption peak appears. The computation model developed here allows us to investigate the absorption of laser radiation in the expanding plasma in full detail.

Let us present typical examples of the solutions obtained. First of all note that we relied on the experiments of Refs [3, 5, 7] in the development of the computation model of absorption and used the laser radiation parameters given in these papers. In this case, the possible existence of a preplasma at the surface of a solid target was disregarded. This assumption is supposedly valid for the experiments of Refs [5] and [7] (the contrast ratio above 10^7 one picosecond prior to the peak of the pulse) but holds not so good for Ref. [3]. The authors [3] assume the existence of a thin preplasma which, in their opinion, can only slightly distort the results of interaction with the solid target.

Fig. 2 shows the distribution of the energy absorbed in the aluminium target plasma irradiated at an angle of 50° by a $\sim$ 200-fs laser pulse, 93 % of the pulse intensity being accounted for by the p-polarised radiation and 7 % by the s-polarised radiation. The total intensity is $I = 2.5 \times 10^{15}$ W cm^{-2}. A maximum absorptivity recorded under these irradiation conditions in the experiments of Ref. [3] was $\sim$ 60 %.

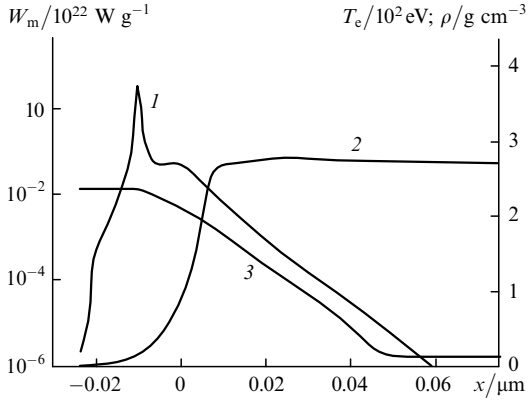

Figure 2. Profiles of the absorbed power of p-polarised laser radiation W_m (*1*) in an aluminium plasma, the plasma density ρ (*2*), and the electron temperature T_e (*3*) at the point in time $t = 100$ fs after the onset of the pulse.

Fig. 2 exhibits a distinct resonance absorption peak observed at the critical-density point. According to the calculation, the absorptivity of a target irradiated at an angle of 50° is about 66 %, which is close to the experimental value. In this case, the resonance absorption, i.e., the absorption related to the field component E_x collinear with the density gradient amounts to $\sim$ 44 %, while the absorption due to inverse bremsstrahlung, for which the component E_y is responsible, accounts for $\sim$ 22 %. This is nearly equal to the absorptivity ($\sim$ 23 %) calculated for the s-polarised radiation beam incident on the plasma at the same angle (50°). This coincidence demonstrates the consistency of description of p- and s-polarised radiation absorption.

Fig. 3 shows the distribution of energy absorbed in the plasma irradiated by the s-polarised laser beam. Except for the polarisation, all the radiation parameters are the same as in Fig. 2. A comparison of these two irradiation versions shows that the resonance peak is missing and the energy release is fairly uniformly distributed in the vicinity of the critical density upon absorption of s-polarised radiation, the absorption taking place in the plasma with both sub- and supercritical density.

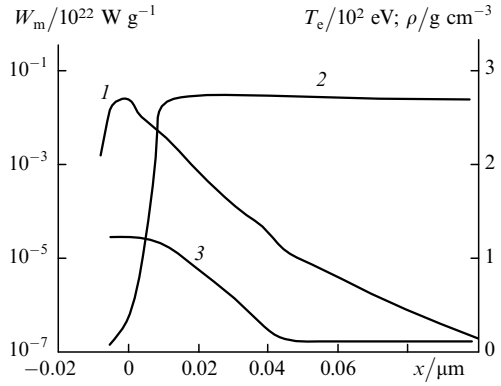

Figure 3. Profiles of the absorbed power of s-polarised laser radiation W_m (*1*) in an aluminium plasma, the plasma density ρ (*2*), and the electron temperature T_e (*3*) at the point in time $t = 100$ fs after the onset of the pulse.

One can see that the maximum absorbed power of the p-polarised radiation exceeds that for the s-polarised radiation by nearly two orders of magnitude. Therefore, numerical simulations reveal a significant difference in the nature of absorption of the p- and s-polarised radiation by the near-surface plasma produced by femtosecond laser pulses.

Figs 2 and 3 also allow one to estimate the characteristic depth δ of field penetration inside the plasma from the width of the absorption region. For the cases considered above, $\delta \simeq 3 \times 10^{-2}$ μm, which exceeds the mean free electron path $[(T_e/m_e)^{1/2}\nu^{-1} \sim 4 \times 10^{-3}$μm] in the absorption region and is indicative of the normal skin-effect mode in the interaction under investigation.

4. Optical properties of the near-surface plasma

To test the theoretical model for the simulation of absorption of a femtosecond pulse of arbitrary polarisation and the method of computer-aided calculations developed by us, we performed the simulations for the values of target irradiation parameters corresponding to the experimental conditions described in the literature [3, 5, 7]. We compared the values of the reflection because this is one of the few parameters of a femtosecond plasma that can be reliably measured in experiments.

In Ref. [7], the absorptivity $A(I)$ of an aluminium plasma was accurately measured. In these experiments, the laser radiation was incident normally to the target surface, which is equivalent to the s polarisation of the beam. Fig. 4 shows the pulse shape $I(t)$, which was measured in the experiments of Ref. [7] and used in our calculations. The laser radiation wavelength was 0.4 μm. The exposure of the aluminium target to the laser radiation with such parameters was simulated in the intensity range $I = 3 \times 10^{14} - 2 \times 10^{17}$ W cm^{-2}. Fig. 5 shows the results of calculations of the aluminium absorptivity $A(I)$ and the experimental points from Ref. [7]. One can

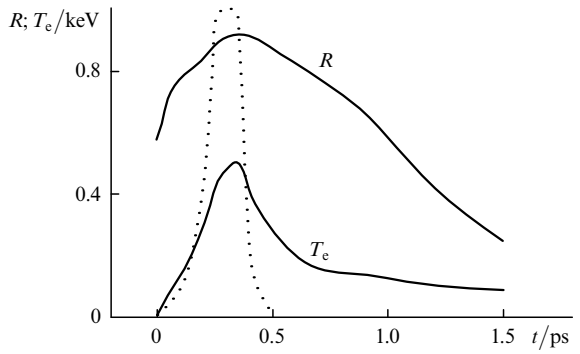

Figure 4. Variation in the reflectivity R and the electron temperature T_e during and after completion of the laser radiation pulse for $\lambda = 0.4$ μm, $\theta = 0^\circ$, and $I = 3 \times 10^{16}$ W cm^{-2}. The dashed line shows the shape of the laser pulse in the calculations and the experiments.

see that the calculated data agree well with the experimental results. In the most interesting intensity range $10^{15} < I < 2 \times 10^{17}$ W cm^{-2}, the maximum difference between the calculations and the experiment does not exceed $\sim 10\,\%$. A reduction in the plasma absorptivity with increasing in intensity of the laser radiation is caused by an increase in the electron temperature and a decrease in the density of the outer layers of the expanding plasma. For $\omega_p \geqslant \omega > \nu$, the absorptivity changes in accordance with the general rules of the normal skin effect [16]:

$$A = 1 - R \sim \frac{2\nu}{\omega_p} \sim \frac{\langle Z \rangle^{3/2} n_i^{1/2}}{T_e^{3/2}}. \qquad (18)$$

For $I \sim 10^{17}$ W cm^{-2}, numerical calculations coincide with the estimates by formula (18) not only qualitatively but also quantitatively.

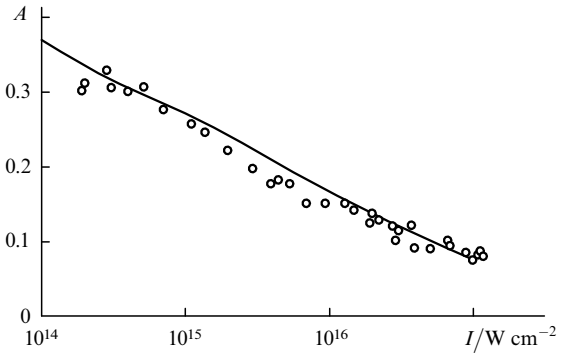

Figure 5. Absorptivity A of aluminium irradiated by laser pulses of different intensity for $\lambda = 0.4$ μm and $\theta = 0^\circ$; the pulse shape is given in Fig. 4, the points represent the experiment of [7] and the solid line represents the simulations.

Based on our calculations, we also studied the variation in the optical characteristics of the near-surface plasma and its other parameters during and after the laser pulse. Fig. 4 presents the relevant information on the reflectivity and the temperature of the expanding plasma produced by a laser pulse with the intensity $I = 3 \times 10^{16}$ W cm^{-2}. One can see that the reflectivity decreases as the plasma expands and cools down. When calculating the reflectivity after termination of the laser pulse, we assumed that the laser radiation intensity was constant and equal to $\sim 10^8$ W cm^{-2} and its absorption did not virtually change the state of the expanding plasma.

The simulations whose results are given in Fig. 5 were carried out without limitation of the heat transfer. The introduction of the heat flux limitation at a level of 0.1 has no effect on the results up to the intensity $I \sim 5 \times 10^{16}$ W cm^{-2}. For $I \sim 10^{17}$ W cm^{-2}, the calculated absorptivity lowers by about 20 %. This is explained by the increase in the plasma temperature during the laser pulse.

Let us discuss the possible role of the light pressure P, which depends linearly on the laser radiation intensity, $P = (1 + R)I(t)/c$, and is therefore manifested at high intensities. For $I \sim 10^{17}$ W cm^{-2}, the peak light pressure is ~ 70 Mbar. Our calculations show that the thermal and dynamic plasma pressure $P_e + P_i + \rho u^2$ at the plasma–vacuum interface amounts to $70 - 100$ Mbar at this intensity and exceeds the light pressure during the entire pulse except, perhaps, a very short period (no longer than tens of femtoseconds) at the onset of the pulse. Therefore, neglecting the light pressure for laser radiation intensities below $\sim 10^{17}$ W cm^{-2} is well substantiated. For higher intensities and longer pulses, the light pressure should be taken into account.

We also used the above computer-aided method of calculations to calculate the reflectivity of the silicon plasma in the intensity range $10^{15} - 10^{17}$ W cm^{-2} measured in Ref. [5]. The pulse duration in these experiments was ~ 160 fs and the laser radiation wavelength was ~ 0.616 μm. Fig. 6 illustrates good agreement between the calculated and measured values of the absorptivity. The experiments were conducted for normal incidence of the laser beam on the silicon target.

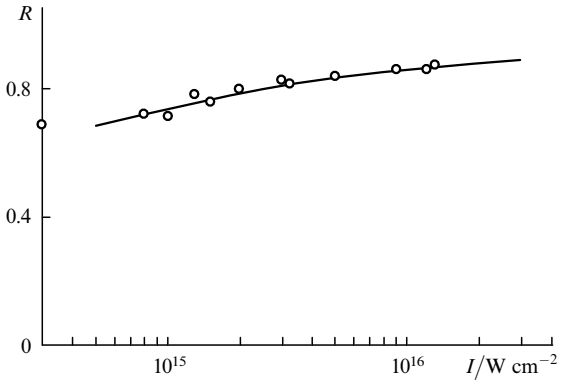

Figure 6. Reflectivity R of the silicon plasma upon irradiation by laser pulses of different intensity for $\lambda = 0.616$ μm, $\theta = 0^\circ$, and $\tau \sim 160$ fs; the points represent the experiment [5] and the solid line represents the simulations.

As already noted, for equal laser pulse intensities and angles of incidence on an inhomogeneous plasma, the absorptivity for p-polarised radiation is higher than that for s-polarised radiation. This was confirmed by a series of calculations simulating the femtosecond laser irradiation. Consider first the time variation of the reflectivity of laser radiation for the plasma, initiated by a laser pulse, during the pulse and after its completion.

Let us compare two cases: an aluminium target irradiated at the same angle $\theta \sim 50^\circ$ by laser radiation pulses ($\lambda = 0.248$ μm, $\tau \sim 200$ fs) of equal intensity $I \sim 2.5 \times 10^{15}$

W cm^{-2} but with different polarisations. Upon completion of the heating pulse, the plasma is exposed to the continuous probing radiation having the same parameters but the low intensity I_{ph}, which does not change the plasma state.

Fig. 7 shows the time dependences of the reflectivities. One can see that the reflectivity for the p-polarised radiation is significantly lower than that for the s-polarised radiation during the pulse and after its completion. The reflectivity for the s-polarised radiation decreases monotonically as the plasma expands and cools down. For the p-polarised radiation, the reflectivity variation pattern proves to be different. This is explained by the fact that the reflectivities for the two radiation polarisations depend on the density gradient scale length L in a different way. The density gradient scale length L can be defined as $1/L \sim (1/n_e)(dn_e/dx)$ at the critical-density point.

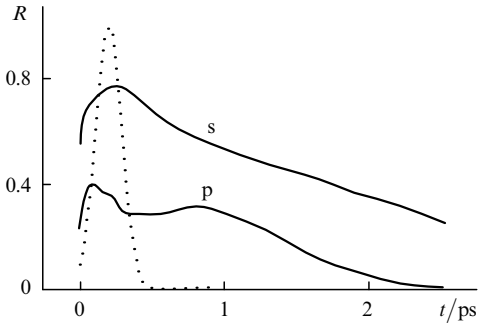

Figure 7. Time dependences of the aluminium plasma reflectivity R for s- and p-polarised laser radiation during the heating pulse and after its completion for $\lambda = 0.248$ μm, $\theta = 50°$, $I = 2.5 \times 10^{15}$ W cm^{-2}, and $I_{ph} \sim 10^8$ W cm^{-2}; the dashed line shows the shape of the laser pulse.

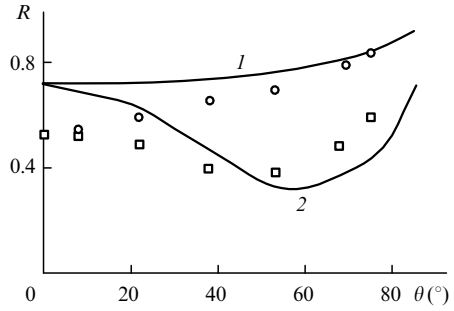

Figure 8. Calculated (solid lines) and experimental [3] (points) reflectivities R of the laser-irradiated aluminium plasma as functions of the angle of incidence θ for $I = 2.5 \times 10^{15}$ W cm^{-2}, $\lambda = 0.248$ μm, $\tau \sim 200$ fs, and different polarisation characteristics of the laser pulse: the s-polarised radiation accounts for 93% of the intensity and the p-polarised radiation for 7% (*1*, ○); the p-polarised radiation accounts for 93 % of the intensity and the s-polarised radiation for 7 % (*2*, □).

Calculations of the reflectivity from a stationary exponential density profile with different gradient scale lengths L showed that the reflectivity for s-polarised radiation decreases monotonically for $L/\lambda \geqslant 0.1$, whereas the reflectivity for p-polarised radiation exhibits oscillations as L/λ varies from ~ 0.1 to unity and then decreases monotonically for $L/\lambda \geqslant 1$. A comparison of the dependences in Fig.8 shows clearly that the s-polarised light is reflected, both during the pulse and after it, much stronger than the p-polarised light, which is due to the resonance absorption.

Fig. 8 gives a comparison of the calculated and experimental [3] reflectivities of the aluminium target irradiated at different angles. The laser radiation in the experiments and the corresponding simulations had a complex polarisation composition. Upon absorption of the p-polarised radiation, strong temperature and energy release gradients appear in the vicinity of the critical density owing to the resonance absorption, as shown in Fig. 2. For this reason, the reflectivities were calculated with inclusion of the thermal flux limitation.

The calculations showed that the limitation affects only the coefficient related to the p-polarised light component. The best agreement between the experiments and the calculations is reached when the thermal flux is limited at a level of 0.5. It is these results that are given in Fig. 8. The minimal reflectivity ($R \sim 38\%$) for the p-polarisation in the experiments was observed for the angle of incidence $\theta \sim 53°$, while in the calculations for $\theta \sim 55°$ ($R \sim 32\%$). A good fit to the experiment as regards reflectivity and the angle of least reflectivity is evident.

The existing discrepancy between the calculated and experimental reflectivities may be caused by the effect of the pre-plasma in this series of experiments. Generally speaking, the pre-plasma is responsible for a reduction in the reflectivity. The inclusion of this factor can lower the calculated reflectivity for s-polarised light in the case under discussion. The ponderomotive pressure and the generation of hot electrons [8] can be disregarded because the parameter $I\lambda^2 \sim 1.6 \times 10^{14}$ W μm^2 cm^{-2} in this case.

In connection with the use of a stepwise plasma boundary model in several papers (see, e. g., Refs [4, 5, 15]), it would be appropriate to determine the limits of validity of this model employing the through calculations of laser irradiation effect. Recall that the stepwise plasma boundary model, assumes that the plasma does not expand during the course of the laser pulse and the energy is released in a material of solid-state density.

To study the question raised above, we considered the ratio between the energy W_{sol} absorbed in the plasma with the unperturbed (solid-state) density and the total absorbed energy W_{tot}. Fig. 9 shows the dependence $W_{sol}(t)/W_{tot}(t)$ for a $\sim$ 170-fs laser pulse for $I \sim 3 \times 10^{16}$ W cm^{-2}. The shape of this pulse and the temperature of the plasma produced by the pulse are shown in Fig. 4. Initially, all the absorbed energy is absorbed by the solid. However, even on the hundredth femtosecond, it accounts for only $\sim 30\%$ of the absorbed energy. By the end of the pulse, its fraction becomes less than $\sim 1\%$. A total of only $\sim 16\%$ of the laser energy absorbed by the target is absorbed in the target material.

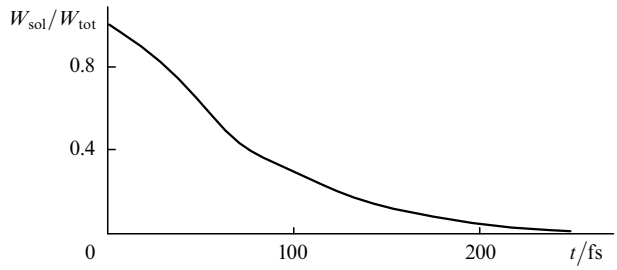

Figure 9. Variation in the fraction of laser radiation absorbed by solid-density aluminium during the laser pulse for $\lambda = 0.4$ μm, $\theta = 0°$, and $I = 3 \times 10^{16}$ W cm^{-2}; the shape of the laser pulse is shown in Fig. 4.

An analysis of the calculations conducted for a laser intensity $I \sim 10^{15} - 10^{17}$ W cm^{-2} showed that from 50 to 90 % of the absorbed energy is absorbed in the expanding plasma with a density below that of a solid. That is why the stepwise boundary plasma model has a limited range of applicability. Even for pulse lengths $\tau \geqslant 50$ fs and the intensity $I \geqslant 2 \times 10^{16}$ W cm^{-2}, the hydrodynamic plasma expansion during the radiation pulse should be taken into account. Under these conditions, the optical parameters of the near-surface plasma should be calculated through the simultaneous solution of hydrodynamic and Maxwell electrodynamic equations.

5. Conclusions

Therefore, the model used here yields a satisfactory agreement between experimental and calculated optical and hydrodynamic characteristics of a femtosecond plasma upon the numerical simulation of solid-target irradiation by a laser pulse of arbitrary polarisation during and after completion of the pulse with an intensity of $\sim 10^{15} - 10^{17}$ W cm^{-2}.

Acknowledgements. This work was supported by the International Science and Technology Centre, Project No. 021.

References

1. Akhmanov S A, in *Itogi Nauki i Tekhniki, Ser. 11Sovremennye Problemy Lazernoi Fiziki'* (Reviews of Science and Technology, 'Contemporary Problems of Laser Physics' Series) (Moscow: VINITI, 1991) vol. 4, p. 5
2. Perry M D, Mourou G *Science* **264** 917 (1994)
3. Fedosejevs R, Ottmann R, Sigel R, et al. *Phys. Rev. Lett.* **64** 1250 (1990)
4. Kieffer J C, Audebert P, Chaker M, et al. *Phys. Rev. Lett.* **62** 760 (1989)
5. Murnane M M, Kaptane H C, Falcone R W *Phys. Fluids B* **3** 2413 (1991)
6. Kolchin V V *Izv. Ross. Akad. Nauk Ser. Fiz.* **56** 67 (1992) [*Bull. Russ. Acad. Sci. Ser. Phys.* **56** (9) 1331 (1992)]
7. Price D F, More R M, Walling R S, et al. *Phys. Rev. Lett.* **75** 252 (1995)
8. Ng A, Celliers P, Forsman A, More R M, Lee Y T, et al. *Phys. Rev. Lett.* **72** 3351 (1994)
9. Andreev N E, Veisman M E, Kostin V V, Fortov V E *Teplofiz. Vys. Temp.* **34** 379 (1996) [*High Temp.* **34** (3) 373 (1996)]
10. Vinogradov A V, Shlyaptsev V N *Kvantovaya Elektron. (Moscow)* **14** 5 (1987) [*Sov. J. Quantum Electron.* **17** 1 (1987)]
11. Afanas'ev Yu V, Gamalii E G, Rozanov V B *Tr. Fiz. Inst. Akad. Nauk SSSR* **134** 10 (1982)
12. Zel'dovich Ya B, Raizer Yu P *Elements of Gas Dynamics and the Classical Theory of Shock Waves* (New York: Academic Press, 1968)
13. Vainshtein L A, Sobelman I I, Yukov E A *Excitation of Atoms and Broadening of Spectral Lines* (Berlin: Springer-Verlag, 1981)
14. Ginzburg V L *The Propagation of Electromagnetic Waves in Plasmas* (Oxford: Pergamon Press, 1970)
15. Rozmus W, Tikhonchuk V T *Phys. Rev. A* **42** 7401 (1990)
16. Kondratenko A N *Proniknovenie Polya v Plazmu* (Field Penetration in a Plasma) (Moscow: Atomizdat, 1979)